SISEs for Safe and High-Energy Batteries

Alex João Pinto de Loureiro Himmel
Mestrado em Química
Departamento de Química e Bioquímica
2022

Supervisor
Iuliia Voroshylova, Investigator, LAQV@REQUIMTE

Co-supervisor
Maria Natália Dias Soeiro Cordeiro, Associate Professor,
Faculdade de Ciências


U.PORTO
FACULDADE DE CIÊNCIAS
UNIVERSIDADE DO PORTO

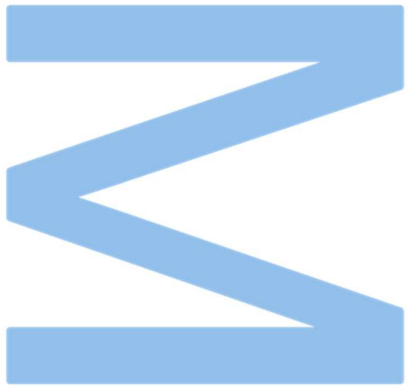

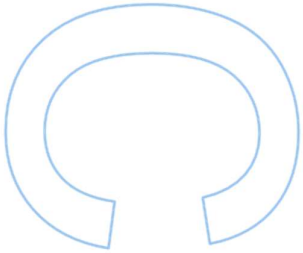

Dedicated to Gustav Adolf Himmel

Sworn Statement

I, Alex João Pinto de Loureiro Himmel, enrolled in the Master Degree Mestrado em Química at the Faculty of Sciences of the University of Porto hereby declare, in accordance with the provisions of paragraph a) of Article 14 of the Code of Ethical Conduct of the University of Porto, that the content of this dissertation reflects perspectives, research work and my own interpretations at the time of its submission.

By submitting this dissertation, I also declare that it contains the results of my own research work and contributions that have not been previously submitted to this or any other institution.

I further declare that all references to other authors fully comply with the rules of attribution and are referenced in the text by citation and identified in the bibliographic references section. This dissertation does not include any content whose reproduction is protected by copyright laws.

I am aware that the practice of plagiarism and self-plagiarism constitute a form of academic offense.

Alex João Pinto de Loureiro Himmel

30th of September 2022

Acknowledgements

The completion of this dissertation was only possible with the help of many people who directly and indirectly contributed to it.

First and foremost, I would like to thank my girlfriend, Catarina, for always being there to listen to me complain when things were not going right and celebrating with me when they were. It is no understatement to say that without her no word of this would be written, as I would probably have quit a long time ago, but her patience and advice kept me going.

I have a huge debt of gratitude to my two supervisors, Iuliia Voroshylova and Natália Cordeiro, whose guidance was instrumental in teaching me all the methods used in this work and how to even approach a work of such magnitude.

With this dissertation and the master's degree it will allow me to achieve, my parents added one more thing in my lifetime debt to them for giving me an education and means to do any and everything I have ever felt inclined to do. Their support and constant check-ups helped tremendously, as well.

My two sisters inspire me every day to be a better professional and a better person and seeing how they were able to navigate complicated moments this past year put everything into perspective and gave me strength in times of need. A huge thank you to their husbands as well for taking loving care of them and always being good role models for me. A word of appreciation goes out to my nephew as well. Frederico, you can't read yet, but when you do I hope you realize that when things get rough, I always think of you, and they get easier.

Finally, I want to thank Elisabete and Nádia for taking the time to teach me certain techniques and always being good company. To all my grandparents, thank you for always remembering me and asking how things were going.

Resumo

Os eletrólitos Solvent-in-salt (SISEs) são uma alternativa recente promissora aos eletrólitos comummente utilizados para baterias e supercondensadores, devido ao seu bom desempenho e segurança melhorada. Uma das baterias mais usualmente disponível é a bateria de iões de lítio, que é capaz de gerar potenciais altos, mas que tem problemas como toxicidade, inflamabilidade e poluição ambiental, por causa dos solventes orgânicos voláteis presentes nas mesmas. Isto leva a que haja uma relutância na utilização destas baterias em áreas emergentes como a dos veículos elétricos. Assim, é de grande importância o desenvolvimento de SISEs como alternativa a estes solventes problemáticos.

As simulações de dinâmica molecular são um método computacional de modelar sistemas microscópicos através do cálculo dos movimentos físicos dos átomos e moléculas que os constituem. Com ajuda deste método, é possível prever as interações entre partículas em sistemas complexos de iões e moléculas com alta precisão, dependendo do campo de forças que é utilizado.

Neste estudo foram utilizados quatro solventes para o sal bis(trifluorometanosulfonil)imida de lítio (LiTFSI): carbonato de propileno (PC), dimetilcarbonato (DMC), trimetilfosfato (TMP) e 1,4-dimetoxibutano fluorado (FDMB). Foram estudadas duas concentrações de LiTFSI: uma diluída, semelhante à utilizada em baterias existentes (~2-3 mol L^{-1}) e uma concentrada, que representa os SISEs (~ 4-6 mol L^{-1}). Os resultados das simulações para ambas as concentrações são discutidos e a interface destes sistemas com elétrodos carregados de grafeno é também explorada. As soluções concentradas apresentam valores mais baixos para condutividade do que as diluídas, mas as propriedades significativas para a sua segurança são mais promissoras (p. ex. viscosidade).

Palavras-chave: Dinâmica molecular, Eletrólitos Solvent-in-salt, Bateria; Armazenamento de energia; propriedades estruturais; LiTFSI; Interface; Orientação ião-molécula; viscosidade; RDF

Abstract

Solvent-in-salt electrolytes (SISEs) have emerged as a promising alternative to the presently used electrolytes for batteries and supercapacitors, featuring high performance and improved safety. Indeed, one of the most common types of currently available batteries are the Li-ion-based ones which can generate high potentials. However, due to the use of volatile organic solvents, these batteries are associated with several problems such as toxicity, flammability, and environmental pollution. This leads to a reluctance in implementing them in such quickly developing and of urgent demand areas, as electric vehicles. Thus, the replacement of toxic and flammable electrolytes with SISEs can be of major importance.

Molecular Dynamics (MD) simulation is a computational method to model microscopic systems through calculation of physical movements of atoms and molecules. It can predict and rationalize the inter-particle interactions in complex ion-molecular systems with high accuracy, depending on force field used.

In this study four different solvents for lithium bis(trifluoromethanesulfonyl)imide (LiTFSI) were addressed: propylene carbonate (PC), dimethyl carbonate (DMC), trimethylphosphate (TMP) and fluorinated 1,4-dimethoxybutane (FDMB). Two LiTFSI concentrations were studied: a diluted one, like the ones already employed in Li-ion batteries (~2-3 mol L^{-1}) and a concentrated one, representing SISE (~ 4-6 mol L^{-1}). The results for both concentrations are discussed. The interface of these systems with charged graphene electrodes is also explored. The concentrated solutions present lower conductivity values than the diluted ones, but the most significant properties pertaining to their safety are more promising (i. e., viscosity)

Keywords: Molecular dynamics, Solvent-in-salt electrolytes, Battery; Energy Storage; Structure properties; LiTFSI; Interface; Ion-molecular Orientation; Viscosity; RDF.

Table of Contents

List of Tables

List of Figures

List of Abbreviations

CAGR	compound annual growth rate
DMC	dimethyl carbonate
EC	ethylene carbonate
FCUP	Faculty of Sciences of the University of Porto
FDMB	fluorinated 1,4-dimethoxybutane
FF	force field
LiFSI	lithium bis(fluorosulfonyl)amide
MD	molecular dynamics
ns	nanosecond
OPLS-AA	optimized potentials for liquid simulations - all atom
PC	propylene carbonate
RDF	radial distribution function
SEI	solvent electrolyte interphase
SISE	Solvent in salt electrolyte
TFSI	Bis(trifluoromethanesulfonyl)imide
TMP	trimethyl phosphate
UP	University of Porto
USD	united states dollars

1. Introduction

The battery industry is one of the fastest-growing economic sectors in the world, owing its growth to the increasing popularity of consumer electronics and electric vehicles. Its market size "was valued at USD 108.4 billion in 2019 and is expected to grow at a compound annual growth rate (CAGR) of 14.1% from 2020 to 2027."[1] The growth of these industries has caused the value of batteries to increase dramatically and the fight to create the best ones is very competitive, with companies like GS Yuasa International Ltd.[2] and BYD Co. Ltd.[3] at the forefront. Due to this growing demand, the stress on resource acquisition is growing and these resources are becoming scarcer.[4]

One of the biggest problems with modern batteries is their safety, as there have been many cases of malfunction leading to accidents such as explosions and fires. In 2016 Samsung released its Samsung Galaxy Note 7 cell phone with a 3.85 V, 3500 mAh Li-ion battery. Because of design flaws (susceptibility to bending around the edges), Samsung users started reporting cases of overheating and exploding batteries. This caused many cell phones to be recalled and, in the end, Samsung was forced to take the Samsung Galaxy Note 7 off the market, due to its lack of security. All together these mistakes and their consequences led to the loss of an estimated 17 billion dollars in revenue.[5] This example underlines the importance for both consumers and companies to build not only more efficient and cheaper batteries, but especially safer ones that can withstand any malfunctions that they may encounter.

Electrolytes are the key component for the safety and high-performance of a battery- They are expected to have certain properties which potentiate these aspects: a large electrochemical window (low melting point - high boiling point), fast transport of ions (high self-diffusion coefficients), chemical and electrochemical stability, high conductivity, and formation of a solid electrolyte interphase (SEI).[6] The most common electrolytes used in Li-ion batteries are non-aqueous solutions, with Lithium hexafluorophosphate ($LiPF_6$) salt dissolved in organic carbonates, like ethylene carbonate (EC), dimethyl carbonate (DMC) or propylene carbonate (PC). These solutions, however, are unstable in high-voltage environments. Another challenge is the formation of the solid electrolyte interphase (SEI), which needs to be optimized to improve "battery performance, irreversible charge loss, rate capability, cycle ability, and safety".[7]

Salt concentration in the context of electrochemistry is one promising aspect which can be studied to find compromises between high-performance and high security. Suo et al [8] showed that Solvent-in-salt electrolytes – meaning solutions with very high salt

concentrations – have very high safety performance, due to the suppression of lithium dendrite growth, as well as a change in the shape of the anode. In another study, Zeng et al[9] concluded that the high-concentration solutions used "display comparable electrochemical performance to that of conventional carbonate electrolyte but have enhanced safety performance".

Molecular dynamics (MD) is a computer simulation technique that numerically integrates Newton's equations of motion for an interacting system with "a specific interatomic potential defined by an initial condition and boundary condition" and is thus able to predict its evolution in time[10]. This means it is a method which studies the position and movement of nanoscale systems and can extrapolate thermodynamic and structural properties on a macroscale. Due to its simulation-based nature, MD is a more ecological and less material-consuming way to study systems which would otherwise be either too expensive or too dangerous to study. Moreover, owing to the proliferation of high-performance computing solutions, MD simulations have become a viable methodology to study even complex systems with an increasing number of molecules and in an increasingly greater timeframe.[11] With the creation of ReaxFF[12] and other force fields (FFs) capable of modelling chemical reactions, the potential applications of this method are growing both in number and in scope. Yang et al [13] show the different computational methods that are used for electrochemistry, of which molecular dynamics is one of the most important ones for "modelling electrochemical interfaces" and "investigating electrochemical reactions at the atomic scale". Figure 1 shows a schematic view of a MD algorithm, which begins by creating a model of the system obtained from experimental or other simulated data. Potential energy is deduced from the molecular structure and the forces, which act on every atom, are obtained from the force-field equations. It is then possible to calculate accelerations and velocities using Newton's laws of motion, from which the updated positions of the atoms can also be taken. These are then used to calculate the new potential energies, which starts the process over, making this an iterative cycle.

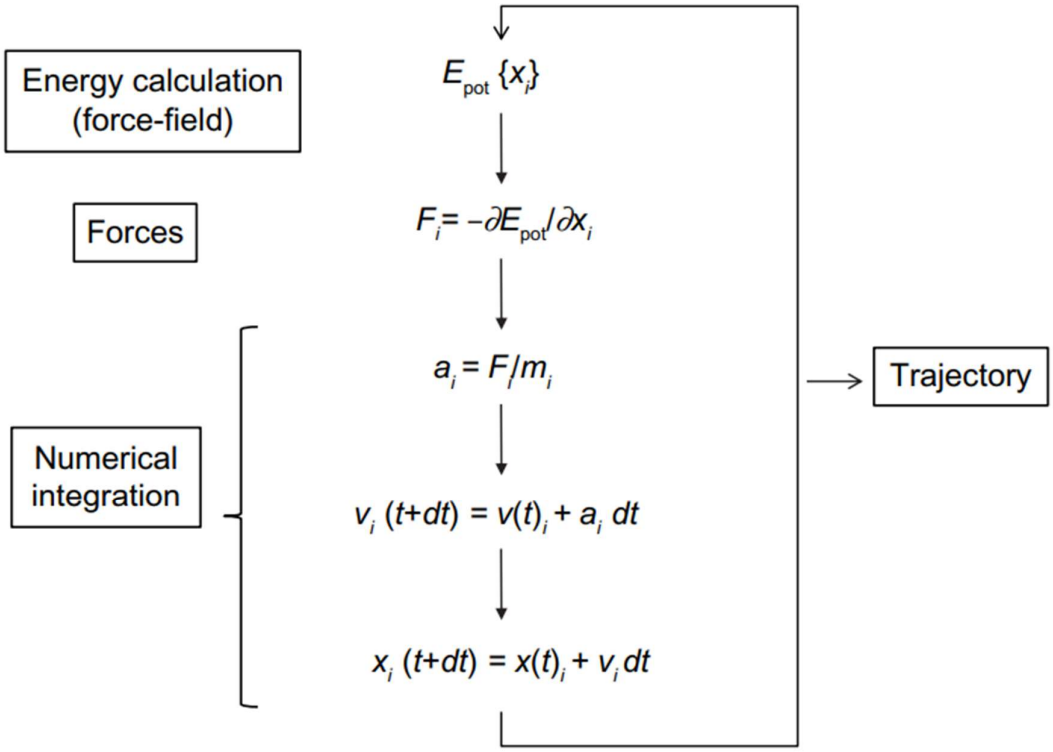

Figure 1: Schematic view of the formulas used in MD calculations[11]

The main method used in this work is MD simulations, and in the heart of any classical MD simulation lays a FF. Force field is a conjunction of equations and associated constants designed to reproduce molecular geometry and properties of substances. Among all the available FFs, the general Optimized Potential for Liquid Simulations (OPLS) all-atom (AA)[14, 15] were chosen for all the studied systems taking into account its general good performance in liquid systems, availability of parameters for a great variety of structures, and thus, transferability to other systems of possible interest. In this work four different solvents for LiTFSI (Figure 2a) were addressed. Propylene carbonate (PC) (Figure 2b) is a cyclic molecule which is polar and aprotic. It was chosen for its wide electrochemical window, high dielectric constant and low viscosity.[16]

Dimethyl carbonate (DMC) (Figure 2c) is a *green* reagent. It presents low toxicity, low viscosity (due to being a linear molecule) and a high conductivity. It is volatile and flammable, which poses an issue when used in batteries; however, this can theoretically be mitigated with an increase in salt concentration. Furthermore, it is biodegradable and cheaper to produce than most carbonates.[16]

Trimethyl phosphate (TMP) (Figure 2d) was chosen due to its high dielectric constant, low viscosity, wide operating temperature range, high flash point, electrochemical stability, good solubility, and low cost. All of these properties make it a suitable compound to be used in safer batteries.[17]

Fluorinated 1,4-dimethoxybutane (FDMB) (Figure 2e) is a solvent which has been studied in recent years as a safer alternative to commonly used organic systems. Yu et al [18] showed that Li-F interactions when using a 1M LiFSI/FDMB system help the solvent to achieve "Li metal compatibility and high-voltage stability." It also presents high Coulombic efficiency, fast activation (over 99% within 5 cycles) and oxidative stability over 6 V.

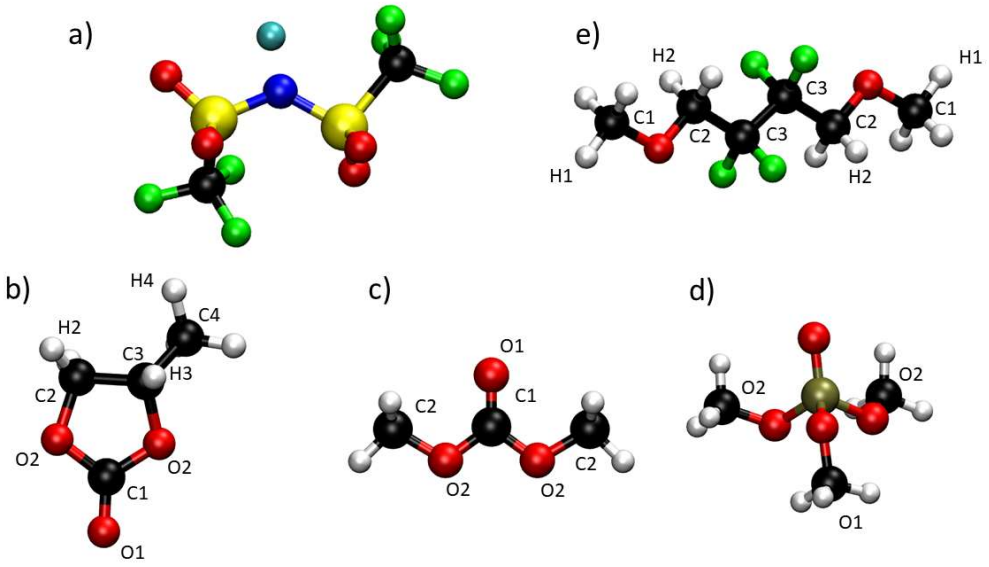

Figure 2: Optimized geometries along with the atom types used throughout the work for a) LiTFSI; b) PC, c) DMC, d) TMP, e) FDMB; nitrogen, carbon, hydrogen, fluorine, phosphorus, sulphur, oxygen and lithium atoms are represented by blue, black, white, green, brown, yellow, red and cyan spheres, respectively.

2. Systems and Methods

2.1 Quantum mechanics calculations

First of all, quantum mechanics calculations were used to optimize the geometry of the studied solvent molecules and TFSI anion, and to access their partial charges distribution. Accurate partial charges may help to improve performance of general FF, used in the study.

To perform the quantum mechanics calculations toward obtaining the partial atomic charges for each solvent, the Gaussian 09[19] package was used. For PC and DMC, a MP2/aug-ccPVTZ basis set was chosen; for TMP, FDMB and the anion TFSI the MP2/aug-ccPVDZ basis set was instead chosen, due to the more complicated nature of these molecules. The results of these quantum mechanics calculations are in the Tables 1-4.

Table 1: Charges obtained by quantum mechanics calculations for PC

Atom Name	Average charge
O1	-0.61472
C1	0.98612
O2	-0.48596
C3	0.34960
C2	0.22147
H3	0.01796
C4	-0.38161
H2	0.03065
H4	0.11060

Table 2: Charges obtained by quantum mechanics calculations for DMC

Atom Name	Average charge
H1	0.04571
C2	0.12229
O2	-0.48411
C1	1.09559
O1	-0.64621

Table 3: Charges obtained by quantum mechanics calculations for TMP

Atom Name	Average charge
P1	1.17111
O2	-0.39995
O1	-0.66935
C1	0.06940
H1	0.05443

Table 4: Charges obtained by quantum mechanics calculations for FDMB

Atom Name	Average charge
C1	-0.04123
H1	0.06981
O1	-0.31878
C2	0.12993
H2	0.07254
C3	0.37679
F1	-0.250614

Table 5: Charges obtained by quantum mechanics calculations for $TFSI^-$

Atom Name	Average charge
N	-0.67635
S	1.09525
O	-0.59029
C	0.55208
F	-0.20953

2.2 Systems

The studied systems, which may be divided into diluted and concentrated ones, comprised a varying number of molecules and, therefore, of interacting sites. The composition of the MD simulation cells is presented in Table 6. Visual comparison of diluted and concentrated systems on the example of LiTFSI-DMC ones are provided in Figure 3.

Table 6: Composition of the simulated systems

System	Concentration/ mol dm^{-3}	Molecules of salt	Molecules of solvent	Number of interacting sites
Diluted PC	0.83	240	960	16 320
Concentrated PC	3.3	600	600	17 400
Diluted DMC	0.83	240	960	15 360
Concentrated DMC	3.3	600	600	16 800
Diluted TMP	0.75	240	960	20 160
Concentrated TMP	3.0	600	600	19 800
Diluted FDMB	0.67	240	960	24 960
Concentrated FDMB	2.7	600	600	22 800

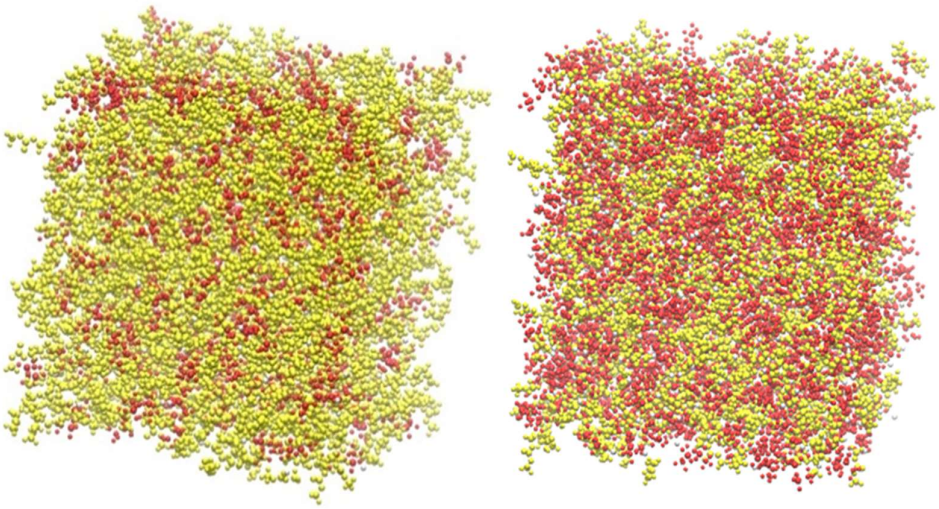

Figure 3: Visualization of two particle boxes. On the left, the diluted DMC system; and on the right, the concentrated one, with the yellow particles representing DMC and the red particles representing $TFSI^-$

2.3 Computational setup

MD simulations were carried out for the systems described above with the GROMACS 2020.4 [20] software package, using the NaRIBaS scripting framework.[21] The initial systems were placed randomly in a cubic box with periodic boundary conditions with the help of the Packmol software.[22] Initially, an energy minimisation run was carried out with the steepest descent method, followed by a short (100 ps) run in the canonical (NVT) ensemble for system relaxation purposes. This was followed by two equilibration runs in the isothermal-isobaric (NpT) ensemble, first for 1 ns using the Berendsen barostat [23] and a time constant of 0.5 ps, and after that for 5 ns employing the Parrinello-Rahman barostat [24] and a time constant of 2 ps. Both runs used a timestep of 1 fs and the pressure was maintained fixed at 1 bar. Finally, two production runs were performed for each system in the NVT ensemble, one during 50 ns, to sample trajectory for dynamic properties estimation, and the other one during 2 ns, to sample trajectory for structural properties calculation. To preserve the temperature, the Nosé-Hoover thermostat [25, 26] was used with a coupling constant of 0.8 ps throughout all simulation steps. Thermodynamic, transport, and structural properties were computed from the simulated trajectories. All simulated properties were compared, whenever possible, with experimental data.

For validation of the FFs, the MD study of pure solvents was conducted in a similar manner, with some exceptions. The relaxation run was deemed not necessary and thus skipped and only one run was performed for both equilibration and production, as opposed

to the two described above. Furthermore, the simulation was conducted for 1.5 ns, but the first 500 ps were considered equilibration and thus not taken into account while estimating the properties.

Carbon plates with body-centred cubic (110) faces were set up in 4 layers using 720 carbon atoms, with the help of the Atomic Simulation Environment (ASE).[27] The graphene plates were approximately squared, with *x* and *y* dimensions of approximately 4 nm by 4 nm and were put on either side of rectangular prisms containing the 1200 molecule systems described above. The MD simulations of these systems containing electrodes were done in a similar fashion as the ones without electrodes, always in NVT ensemble. The first energy minimization run was equal, *i.e.,* by resorting also to the steepest descent method. The second step was an equilibration run of 0.1 ns, with a time step of 1 fs. The velocity rescaling thermostat was used for holding fixed the temperature[28]. The following step was the charging of the electrodes, which was carried out for 2 ns, with a time step of 1 fs. To charge the electrodes, an electric field (E) was applied to the simulation box in the *z*-direction, perpendicular to the electrodes. The equation relating the electrical field with the electrode surface charge is as follows: $E = \sigma\varepsilon_0^{-1}\varepsilon^{-1}$, where ε_0 represents the vacuum permittivity and $\varepsilon = 1$ the high-frequency permittivity of the system. The surface charges used were 0, 2, 4, 8, 12 and 16 μC cm^{-2}. Finally, the production run lasted for 10 ns. An example of such a system can be seen in Figure 4.

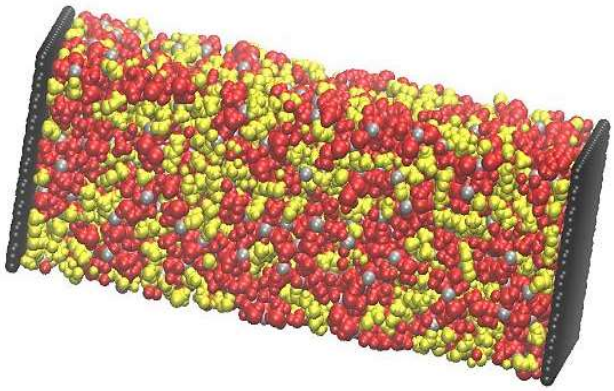

Figure 4: Visualization of a simulation box with SISE, confined between two electrodes. The system is the concentrated DMC-LiTFSI one. DMC molecules, $TFSI^-$ anions, Li^+ cation and graphene plates are yellow, red, silver, and black, respectively

2.4. Properties calculation

Density is the ratio between the mass of solute in a solution and the volume of the entire solution. In practical sense, this means that the density measurement shows how many ions there are in the solution, and it is logically expected that as the concentration of

the solution increases, so does its density as they are proportional to each other (concentration being the ratio between number of molecules of solute *vs.* the volume of the solution). Density, *d*, was obtained from GROMACS built-in tools after the equilibration calculations of the bulk systems.

Viscosity is a measure of the resistance of a fluid to changes in shape which is caused by internal friction between molecules.[29] Shear viscosity was calculated from the transverse current autocorrelation functions[30] through the formula: $\eta(k) = \eta_0 (1 - a k^2)$ (where η represents the shear viscosity and k represents the wave vectors).

Self-diffusion represents the flux of particles "in the absence of a chemical potential gradient". [31] To obtain the self-diffusion coefficients, *D*, the Einstein relation,

$$D = \frac{1}{6} \lim_{t \to \infty} \frac{d}{dt} \langle |r_i(t) - r_i(0)|^2 \rangle, \quad (1)$$

was used, where r_i is the vector coordinate of particle *i* at time *t*.

Enthalpy of Vaporization. Enthalpy is an energy-like property determined by the temperature, pressure, and composition of a system.[32] Vaporization enthalpy (ΔH_{vap}) is the amount of heat that must be supplied to a system for it to change states from liquid to gas. ΔH_{vap} was calculated through the equation:

$$\Delta H_{vap} = E_{pot}(gas) - E_{pot}(liquid) + RT, \quad (2)$$

where E_{pot} (gas) and E_{pot} (liquid) are the total energies in the gas phase and in the liquid phase, respectively, *R* is the universal gas constant, and *T* = 298.15 K.

Radial distribution functions (RDFs) describe how selected atoms or molecules' centres of mass position themselves in relation to a specific point of reference. The general expression to calculate RDFs G(r) is:

$$rG(r) = 4 \pi r^2 (\rho(r) - \rho(0)), \quad (3)$$

where $\rho(r)$ is the density of the atoms at distance *r* and ρ (0) is the bulk density of the atoms.[33]

Conductivity, σ, was calculated through the current autocorrelation functions and the correlation of the rotational and translational dipole moment of the system.

Dielectric constant. The dielectric constant, ε_r was obtained through the computation of the total dipole of the system.

3. Results and discussion

3.1 Validation

As a first step of the simulation, the density, viscosity, self-diffusion coefficients and heats of vaporization of pure solvents were used to test the performance of FFs. The results of this step are summarized in Table 7.

Table 7: Literature experimental (lit), and simulated (sim) physicochemical properties of pure PC, DMC, TMP and FDMB solvents at 298.15 K with the respective errors*

Solvents	d / g cm^{-3}			η / mPa s			D / m^2 s^{-1}			ΔH_{vap} / kJ mol^{-1}		
	Lit	Sim	Err (%)	Lit	Sim	Err (%)	Lit	Sim	Err (%)	Lit	Sim	Err (%)
PC	1.20	1.23	2.1	3.0	2.2	-27	0.52	0.08	-84	61.5	73.4	19
DMC	1.06	1.06	0.05	0.58	0.64	9	2.8	1.21	-57	38.0	43.2	14
TMP	1.21	1.22	0.72	1.3	1.2	-6		0.46			64.4	
FDMB	1.21	1.28	5.4	1.4	2.6	82		0.08			69.4	

*These and the following references to errors stand for $(X_{exp} - X_{sim})/X_{exp} \times 100$, where X_{exp} is the literature experimental and X_{sim} is the property obtained by simulation in this work.

The table above (Table 7) shows that the FF and methods used can accurately predict characteristics such as density, viscosity, and vaporization enthalpy. The values for the self-diffusion coefficient and some viscosities are less exact, due to the shortcomings of OPLS FFs and the use of a generic FFs (not tuned specifically to these solvents). As for the viscosity of FDMB, a rather distant simulation value may be the result of scarcity of experimental data: indeed, this is a new solvent with only one experimental (may be, somehow problematic) value available. Summarizing, the general reproducibility of the addressed properties is acceptable due to the generic scope of the study which can then be adapted for different situations and solvents.

3.2. LiTFSI-solvent systems: bulk properties.

3.2.1 Structure properties

To probe the molecular structure in LiTFSI-based electrolyte systems it was decided to access the centre-of-mass and atom-atom RDFs, presented in Figures 5-10.

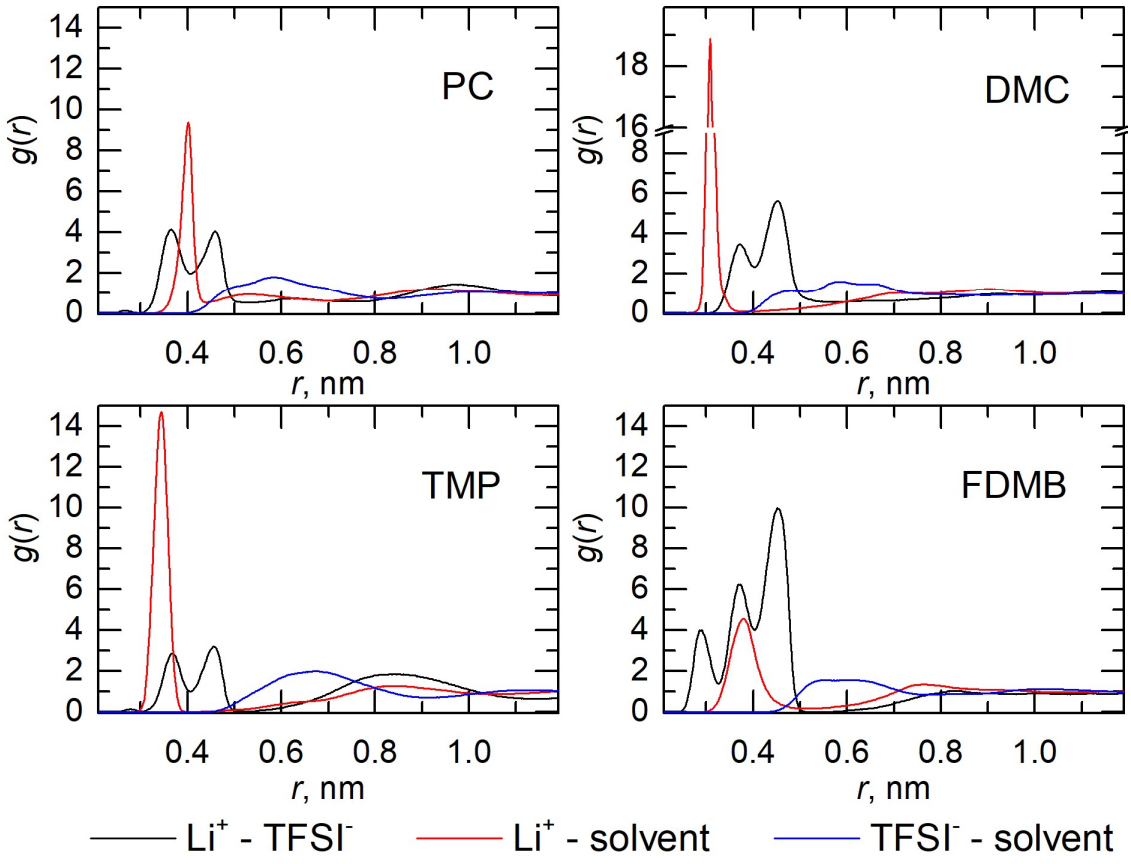

Figure 5: Centre-of-mass radial distribution functions, $g(r)$, in diluted LiTFSI-solvent systems

The figure above shows the radial distribution functions for the centres of mass of molecules and ions in the four different systems of diluted salt concentration. All graphs show three distinct peaks at the distance of 0.5 nm and below, and in all four cases the interaction between $TFSI^-$ and solvent is the least relevant, both in terms of distance and density of atoms. When comparing the relation between Li^+ cations and $TFSI^-$ anions it becomes apparent that the anion forms the first layer of coordination of the cation in the case of systems with PC and FDMB solvents, while getting replaced by the solvent in the cases of DMC and TMP systems. Regarding these layers, the four systems present different positions. For PC, the first and third layers are composed of $TFSI^-$, whilst having a second

layer in between which is where the solvent positions itself. In the system with DMC, the first layer comprises solvent molecules. This system is the only one where the first layer is almost exclusively composed of solvent molecules, which points to a bigger facility of DMC to replace the anion in its relationship with Li. This is most likely due to the flexible nature of DMC. Indeed, this is a relatively small molecule with no impediments like rings, whilst also having the two negative poles of the two oxygen atoms, which heavily attract the cations. TMP is the other solvent which appears in the first layer of the cation; the main difference from DMC is that this layer is shared between TMP and the anion, with a bigger density of TMP atoms and their occurrence slightly closer to the cation than the anion, still however sharing the same layer. Because of this, there is only one more layer formed of anions at the same distance as other third layers in the other systems. With FDMB, anions are present in the three layers, and they share the second layer almost equally with the solvent. Distance-wise all peaks are in the same positions for all solvents, except for the peak of the Li-solvent interaction. It is closest for DMC (≈ 0.31 nm), followed by TMP and FDMB (≈ 0.35 and 0.38 nm, respectively) and the furthest peak is the PC one (≈ 0.4 nm). The TFSI-solvent peak is negligible, both because of the distance between the molecules (≈ 0.6 nm) and the height of the peak.

Figures 6 and 7 show a more precise version of these relationships between molecules where the RDFs are calculated regarding specific atomic sites instead of the centres of mass of the components. It is prominent that the most relevant interactions occur between Li^+ ions and the oxygen atoms of both solvent and anion (in the case of the solvents with more than one oxygen atom, the most relevant one is the one in the carbonyl group, see Figure 2). The second layer is then composed of the other oxygen atoms of the solvent, the nitrogen atoms of $TFSI^-$ and, to a lesser extent, there are some oxygen atoms of $TFSI^-$ in this layer as well. The latter corroborate that, like it was observed above in the centre-of-mass RDFs, there is a second layer of $TFSI^-$ anions to be seen. The existence of a third layer of $TFSI^-$ anions in the system with FDMB is also visible in the atom RDFs, as there are 2 peaks of $TFSI^-$ nitrogen atoms instead of one around 0.4 nm and there is a peak around 0.65 nm of $TFSI^-$ oxygen atoms.

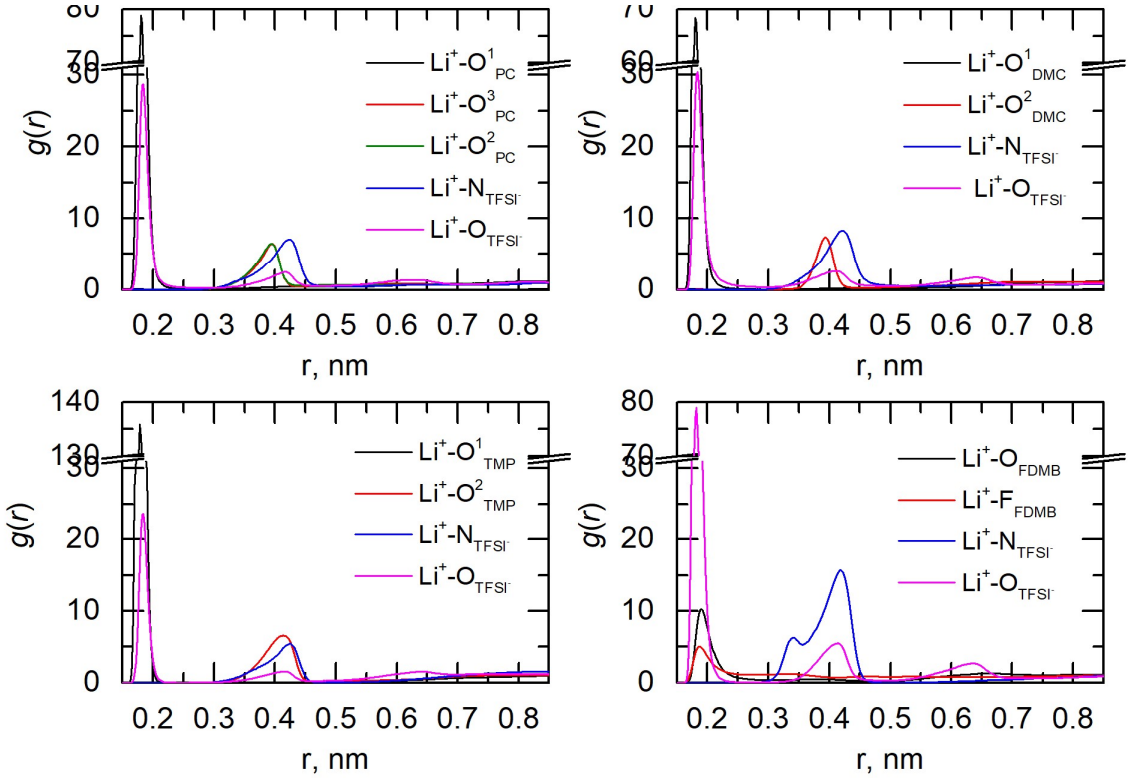

Figure 6: Atom-atom radial distribution functions, *g*(*r*), in diluted LiTFSI-solvent systems

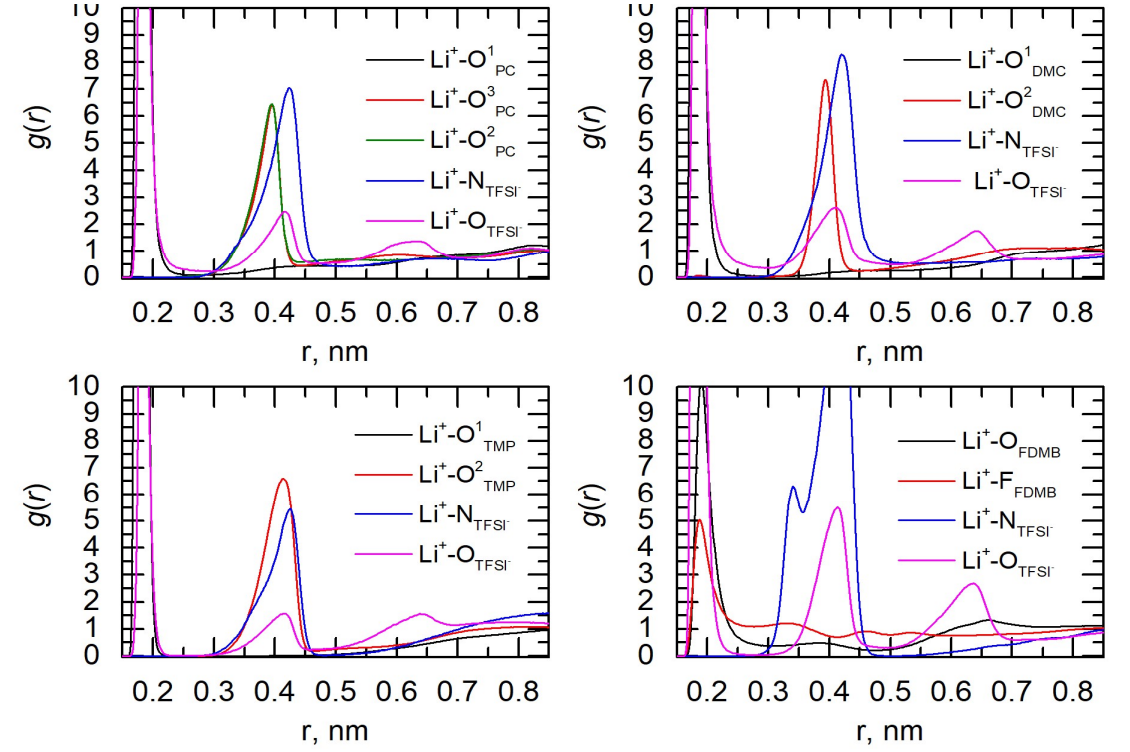

Figure 7: Enhanced radial distribution functions relative to the different atoms of the diluted systems

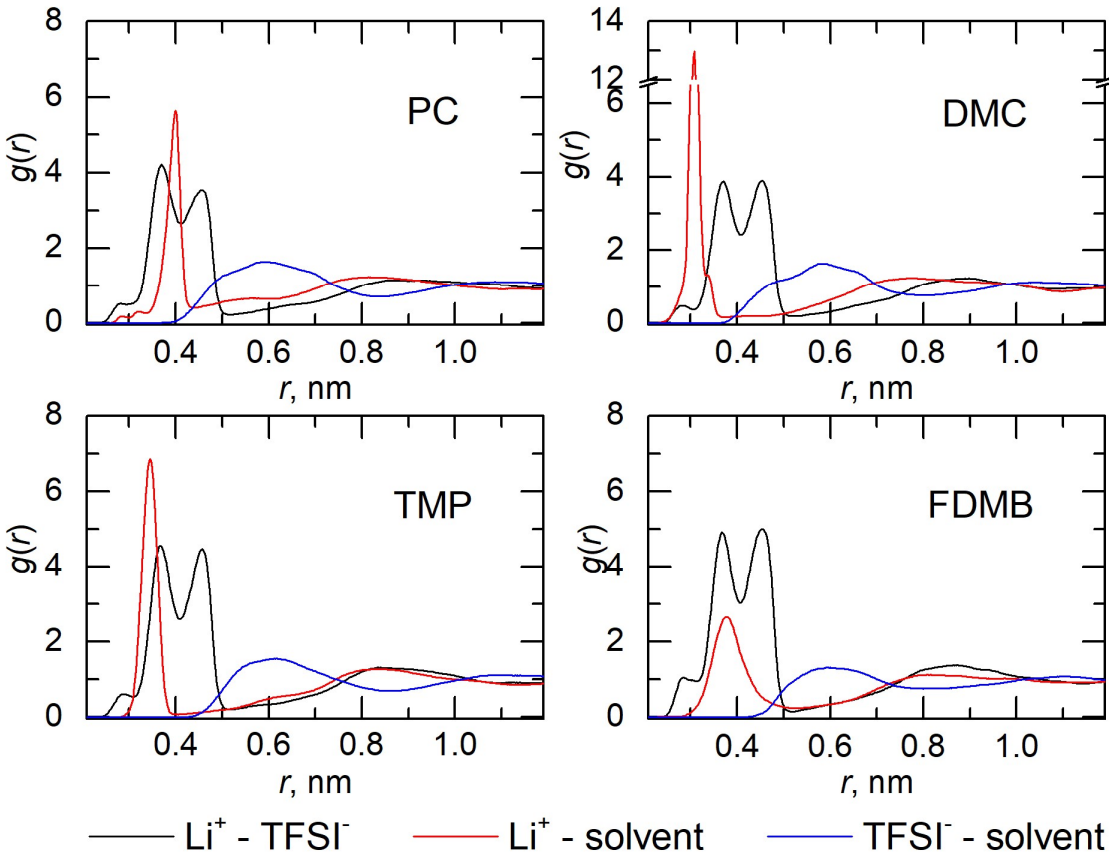

Figure 8: Centre-of-mass radial distribution functions, $g(r)$, in concentrated LiTFSI-solvent systems

In the concentrated solutions, it appears that molecules interact at the same distances as in the diluted ones, so an increase in concentration does not change the distance of cation-anion and ion-molecular interactions. However, the peaks change in height, so the intensity of these interactions is different when the concentration of salt is increased. The closest cation-anion peak (≈ 0.28 nm) which in diluted solutions appeared only on the system with FDMB, is now noticeable in all systems. In fact, it seems that all peaks between Li^+ and $TFSI^-$ are higher than the ones in diluted solutions, which is to be expected upon the increase in concentration. In addition, the two highest peaks for cation-anion interactions in systems with FDMB are closer to each other in height compared to the diluted mixtures, where the third peak is considerably higher. This points to more equal distribution of anions between solvation layers, which is likely due to the lesser competition with the solvent for the closest positions to the cation, because of the higher ratio of anions to solvent. The interaction between anion and solvent continues to be the less meaningful one, as the increase in concentration leads to a lesser density of solvent around the anion. The atom-atom RDF's (Figures 9 and 10) present the same information, analogously to the

diluted ones. The closest and most dense interactions are between Li^+ and the oxygen atoms of both solvent and anion carbonyl groups, followed by a layer formed by nitrogen atoms of the anion and the other oxygen atoms of the solvent. The most striking difference to the diluted RDF's is the presence of a smaller peak of Li-N (TFSI) interaction around 0.35 nm in all systems, while in the diluted ones it is only present for FDMB.

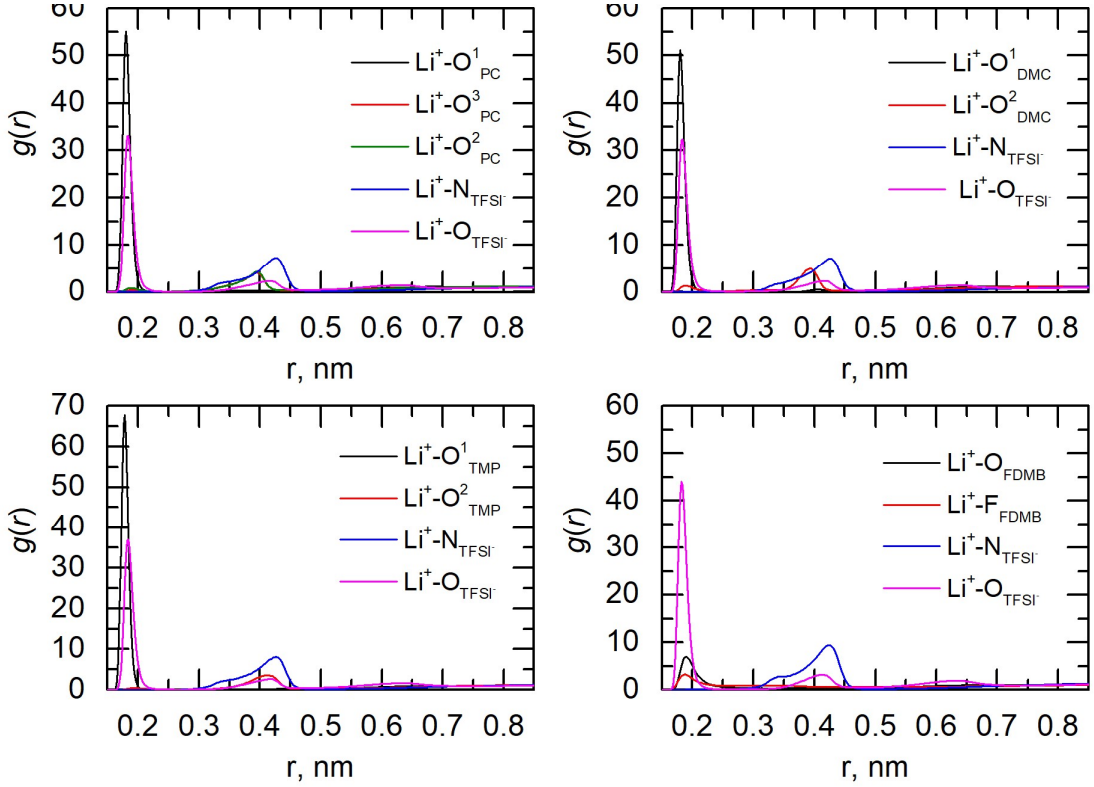

Figure 9: Atom-atom radial distribution functions, $g(r)$, in concentrated LiTFSI-solvent systems

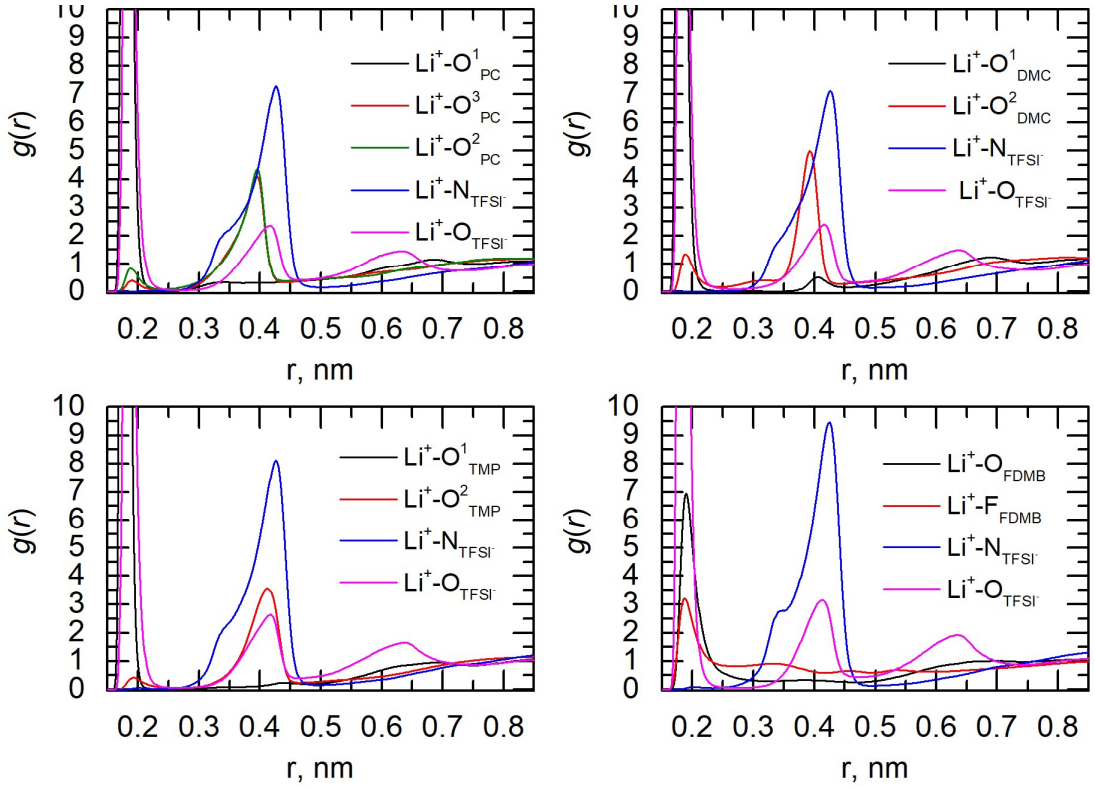

Figure 10: Enhanced radial distribution functions relative to the different atoms of the concentrated systems

3.2.2. Thermodynamic and dynamic properties

Thermodynamic and dynamic properties, calculated for both the diluted and concentrated LiTFSI-solvent systems at 298.15 K from MD simulation trajectories are summarized in Table 8.

Table 8: Literature experimental (lit) and simulated (sim) properties in LiTFSI-solvent systems at 298.15 K with the respective errors in parentheses

		d / g cm^{-3}		η / mPa s		σ / S cm^{-1}		ε_r	D_+ / 10^{-13} m^2 s^{-1}		D_- / 10^{-13} m^2 s^{-1}		D / 10^{-13} m^2 s^{-1}	
PC														
Dil	Sim.	1.51	(15%)	6.43 x 10^{-3}		0.012	(54%)	7.45	5.0	(-100%)	9.0	(-99%)	11	(-100%)
	Lit.	1.31				0.0079			1250		1410		2820	
Conc	Sim.	2.66	(-33%)	5.40		0.0037	(54%)	2.76	7220		13000		23300	
	Lit.	1.78				0.0014								
DMC														
Dil	Sim.	1.44		0.126	(-99%)	0.018	(1400%)	1.56	70		120		470	
	Lit.			53.7		0.0012								
Conc	Sim.	1.74		6.18		0.0036		1.80	1.23		1.90		4.04	
	Lit.													
TMP														
Dil	Sim.	1.45		2.57		0.19		5.75	87		96		131	
	Lit.													
Conc	Sim.	1.75		5.84		0.0079		2.89	1.27		2.13		6.21	
	Lit.													
FDMB														
Dil	Sim.	1.48	(15%)	5.55	(23%)	0.0043	(43%)	19.3	50000		7000		176000	
	Lit.	1.29		4.5		0.003								
Conc	Sim.	1.73		17.0		0.001		5.13	7610		9300		5255	
	Lit.													

Looking at the differences between systems, PC and TMP exhibit similar density, DMC's is the lowest and FDMB's is the highest both in diluted and concentrated solutions. PC's viscosity is the highest, TMP's and FDMB's are similar, and DMC's is the lowest. As for their self-diffusion coefficients, PC and FDMB have similar ones, while both TMP and DMC present higher values. Finally, the dielectric constant for FDMB-containing systems shows the highest value, followed by PC, TMP and DMC.

When comparing the two concentrations, some trends are apparent. As expected, the density is bigger for all concentrated solutions in comparison to their diluted counterparts (1.45-1.50 g cm^{-3} *vs.* 1.74-1.78 g cm^{-3}). This can be explained by the fact that there are more molecules of solute in the solution, thus increasing the ratio between mass of solute per volume of solution. As for the self-diffusion coefficients, they are bigger on the concentrated solution of PC, but in the DMC, FDMB and TMP solutions it is the diluted ones which have higher values (except for the anion in the FDMB solution). Conductivity values are expectedly higher for the diluted solutions, because of the higher amount of solvent to carry

the electric current. Also, the concentrated systems are more viscous due to the higher number of solute molecules which cause internal friction in the fluid. The dielectric constant decreases with the increase in concentration for all solvents except DMC.

Because of these characteristics (lower dielectric constant, higher viscosity, while maintaining good conductivity), concentrated systems are more promising for electrochemical storage and transformation devices. Because of this, the electrode-electrolyte interfaces are of primary interest for these systems.

3.3. SISEs interface with graphene electrodes

The snapshots of the layers, adjacent to the anode and cathode, on the example of the LiTFSI-DMC concentrated system are presented in Figures 11-14 as a function of electrode charge. LiTFSI-DMC system is chosen for this analysis as a typical representative of SISEs, studied here; all the other systems show visually similar structural behaviour.

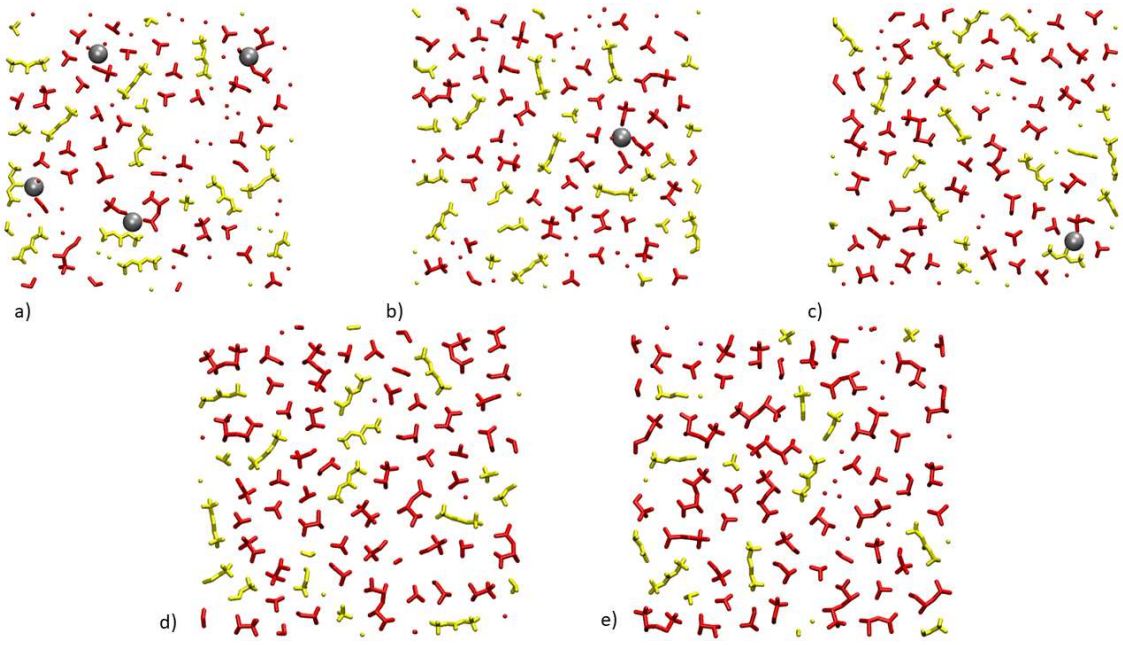

Figure 11: Snapshots of the first layer of the SISE-anode interface in LiTFSI-DMC concentrated system. The point of view is from the anode surface. $TFSI^-$ anions, DMC molecules and Li^+ cations are represented in red, yellow, and silver, respectively. Electrode a) is charged with 0 μC cm^{-2}, b) is charged with 4 μC cm^{-2}, c) is charged with 8 μC cm^{-2}, d) is charged with 12 μC cm^{-2} and e) is charged with 16 μC cm^{-2}

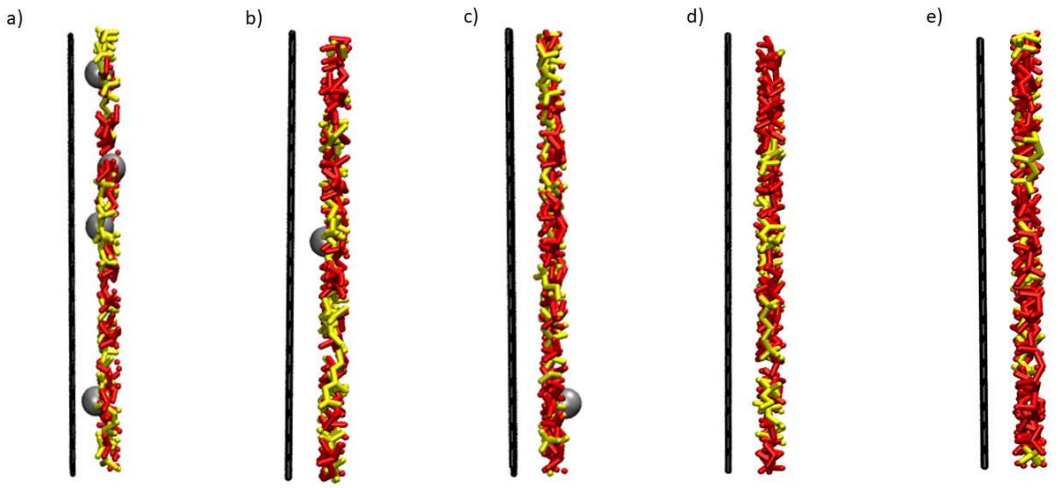

Figure 12: Snapshots of the first layer of the SISE-anode interface in LiTFSI-DMC concentrated system. The point of view is perpendicular to the anode surface. $TFSI^-$ anions, DMC molecules, Li^+ cations and graphene electrode are represented in red, yellow, silver, and black, respectively. Electrode a) is charged with 0 μC cm^{-2}, b) is charged with 4 μC cm^{-2}, c) is charged with 8 μC cm^{-2}, d) is charged with 12 μC cm^{-2} and e) is charged with 16 μC cm^{-2}

The figures above show molecules and ions in the first layer at anode from the point of view of anode and in perpendicular direction. With the increase of electrode charge, one can clearly see the movement of the molecules due to their own charge and internal dipoles. When no charge is present, the molecules are randomly mixed in the box, including the adjacent to electrode surface areas, with interactions as stated above between solvent and ions (especially the cation Li^+ and the negative poles in all the solvents). When charge is introduced, Figures 11 and 12 show how Li^+ cations gradually disappear from the first layer of the anode, as they are pushed away by electrostatic interactions. At the same time, the percentage of $TFSI^-$ anion increases in this first layer, as the negative charge is pulled towards the positive charge of the electrode. When enough charge is introduced (12 μC cm^{-2}, in this case) there are no longer any Li^+ cations in the first layer and the ratio between $TFSI^-$ anion and solvent is favourable to the anion.

On the reverse end, the opposite occurs in the closest to the cathode layer. The increase in charge shows a clear increase in the number of Li^+ ions in the first layer, but the disappearance of $TFSI^-$ is not as great as the disappearance of Li+ at the anode, probably due to $TFSI^-$ being a larger ion with a possibility for a positive pole (on the sulphur and carbon atoms) which would get slightly pulled to the cathode.

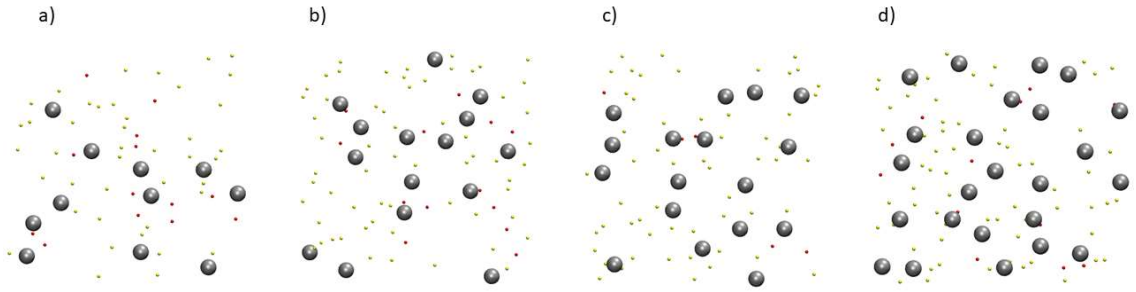

Figure 13: Snapshots of the first layer of the SISE-cathode interface in LiTFSI-DMC concentrated system. The point of view is from the cathode surface. $TFSI^-$ anions, DMC molecules and Li^+ cations are represented in red, yellow, and silver, respectively. Electrode a) is charged with 4 μC cm^{-2}, b) is charged with 8 μC cm^{-2}, c) is charged with 12 μC cm^{-2} and d) is charged with 16 μC cm^{-2}

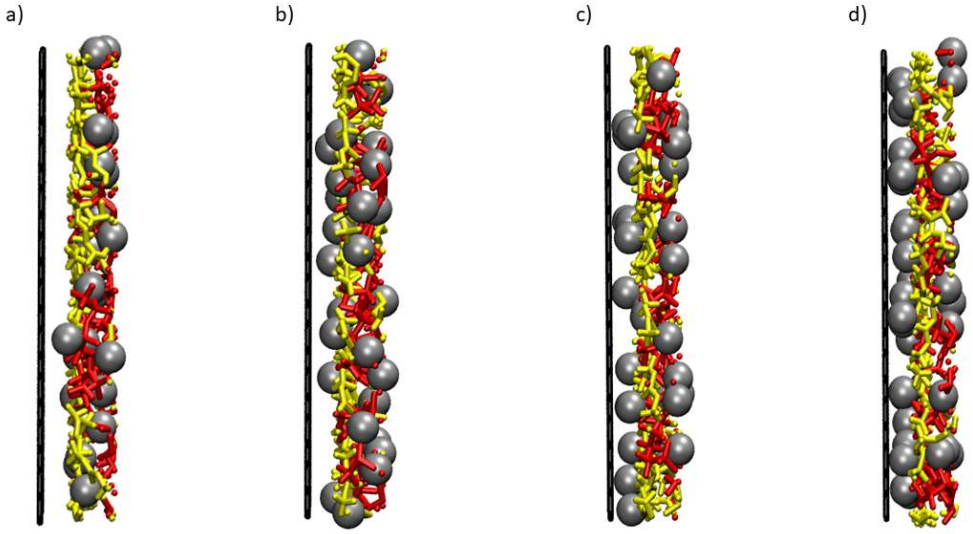

Figure 14: Snapshots of the first and second layers of the SISE-cathode interface in LiTFSI-DMC concentrated system. The point of view is perpendicular to the cathode surface. $TFSI^-$ anions, DMC molecules, Li^+ cations and graphene electrode are represented in red, yellow, silver, and black, respectively. Electrode a) is charged with 4 μC cm^{-2}, b) is charged with 8 μC cm^{-2}, c) is charged with 12 μC cm^{-2} and d) is charged with 16 μC cm^{-2}

The analysis of layering structure of $TFSI^-$ anion and solvent molecules in all studied concentrated solutions was made at 0 and 2 μC cm^{-2} charges. The tilt angles for these systems are defined as the angles between vectors uniting two atoms of a molecule and a unit vector in the *z* direction (this is the vector perpendicular to the graphene/SISE interface

plane). For all systems, two vectors for $TFSI^-$ were additionally calculated: (i) between the two carbon atoms, and (ii) between the sulphur atoms. In the case of PC, the angle calculated was between the plane of the ring and the unit vector described previously. For DMC, two vectors were used, namely: (i) uniting the carbon and oxygen atoms of the carbonyl group and (ii) uniting the other two carbon atoms. For TMP the vector chosen was between the phosphor atom and the oxygen atom in the phosphate group. Finally, for FDMB, the vector used was between the two carbon atoms of the methyl groups. In this analysis three zone next to electrode were distinguished: the first layer, the second layer and the bulk. The layers thickness was defined taking into account the above made visual analysis of layering structure in the vicinity of the electrodes and the geometrical size of the species. Thus, the first and second layers were of the same thickness, namely, 0.5 nm. The result of this analysis is presented in Figures 15-18.

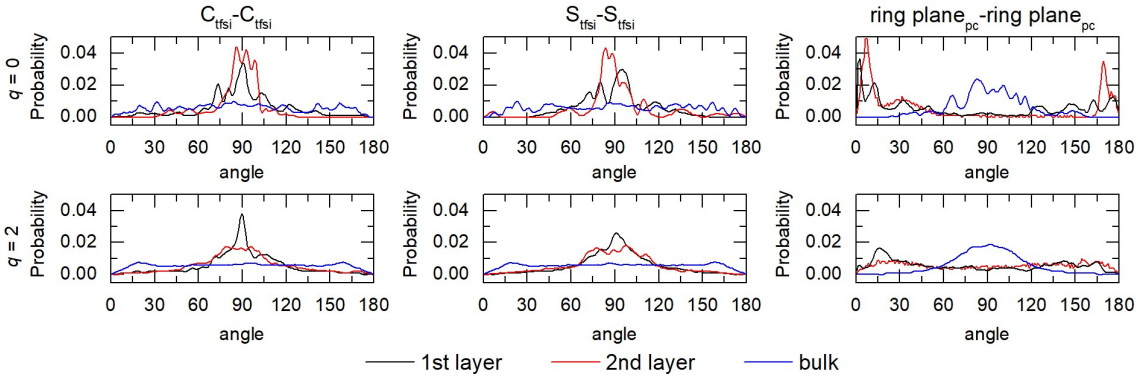

Figure 1515: Normalized tilt axis probability distribution for $TFSI^-$ anions and solvent molecules in the first and second layers of the electrode interface, as well as the bulk PC solution in uncharged (top) and charged with 2 μC cm^{-2} (bottom) systems.

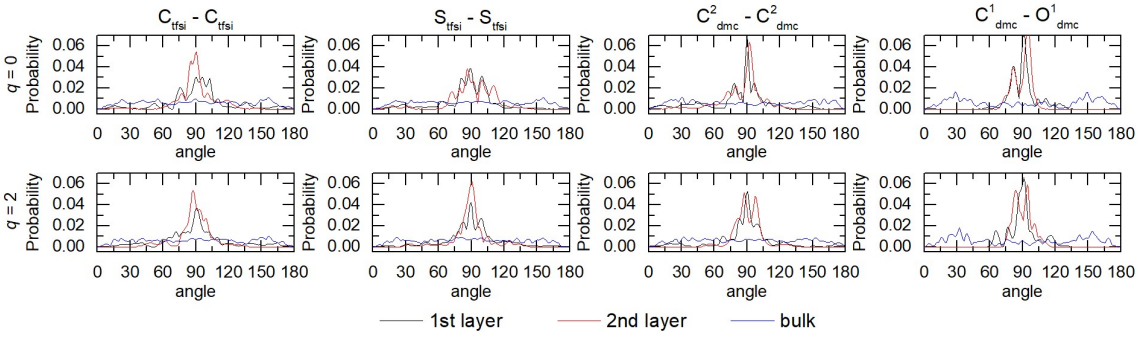

Figure 1616: Normalized tilt axis probability distribution for $TFSI^-$ anions and solvent molecules in the first and second layers of the electrode interface, as well as the bulk DMC solution in uncharged (top) and charged with 2 μC cm^{-2} (bottom) systems.

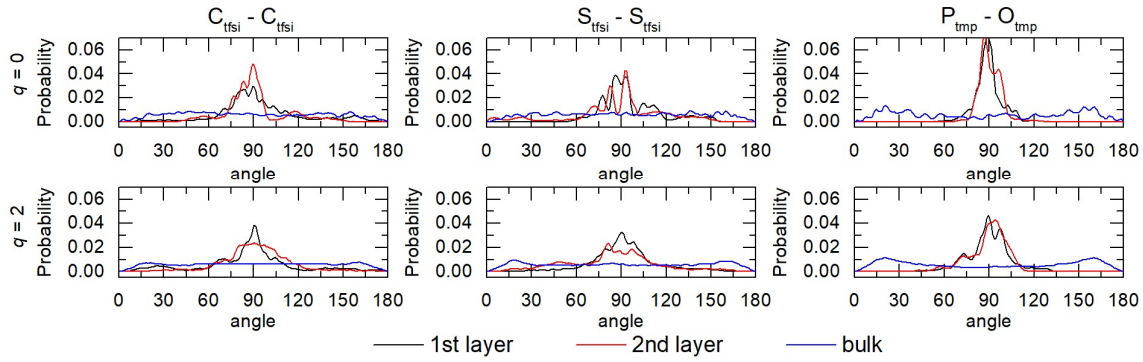

Figure 1717: Normalized tilt axis probability distribution for $TFSI^-$ anions and solvent molecules in the first and second layers of the electrode interface, as well as the bulk TMP solution in uncharged (top) and charged with 2 μC cm^{-2} (bottom) systems.

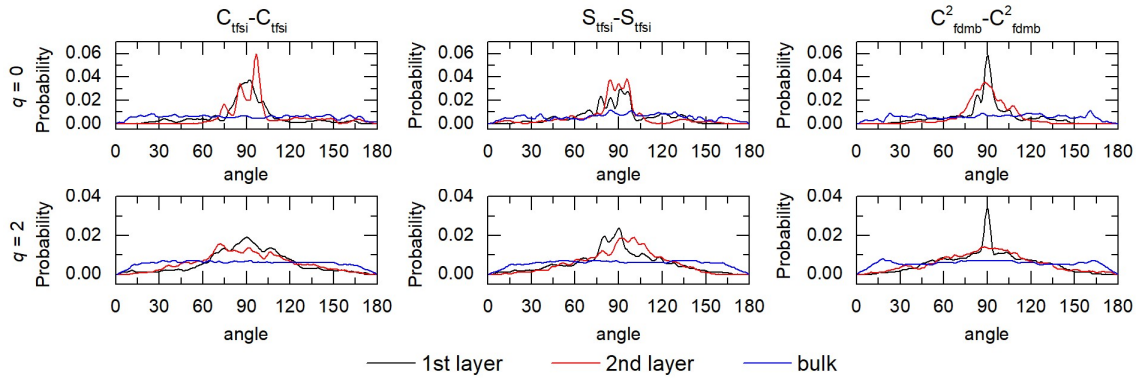

Figure 1818: Normalized tilt axis probability distribution for $TFSI^-$ anions and solvent molecules in the first and second layers of the electrode interface, as well as the bulk FDMB solution in uncharged (top) and charged with 2 μC cm^{-2} (bottom) systems.

Figures 15-18 show the normalized tilt axis probability distribution for selected vectors in the anion and solvent molecules, for all the concentrated systems. It is visible that the $TFSI^-$ anions in the first and second layers position themselves mainly with the sulphur-sulphur and carbon-carbon vectors perpendicular to the normal vector of the uncharged electrode with the biggest peaks being located at 90 degrees, as well as some peaks in the 80-100 degree range. This appears to be true for all the solvents, which reiterates the importance of the interactions between the poles of the solvent molecules and the electrode molecules. These interactions become more apparent when the electrodes are charged, as the peak around 90 degrees becomes more well-defined, while other close peaks become smaller. The second layer follows the same pattern as the first layer, with an even higher disparity between the peaks near 90 degrees, and the probability for the rest of the angles. Inside of the bulk, the TFSI anions position themselves randomly.

As for the solvent molecules themselves, PC's plane of the ring displays a clear preference for parallel orientation with respect to the normal vector of the electrode in the first and second layers, with two big peaks around 0 and 180 degrees, which are softer when the electrodes are charged and in the case of the second layer almost disappear into randomness. The molecules in the bulk exhibit the opposite distribution, as there is a wide peak (or group of peaks) from 60 to 120 degrees.

DMC's two chosen vectors present similar angle probability, as they have big peaks for the first and second layers in the 80-100 degree range, both when the electrodes are uncharged as well as charged. The bulk does not show a clear tendency for the C-C vector, but for the C-O vector of the carbonyl group there are two small peaks around 30 and 150 degrees.

The same behaviour is observed for the phosphate group vector in the system containing TMP and for the C-C vector in FDMB, which also display the considerable peak in the first two layers around 90 degrees and two small peaks in the bulk, at 20 and 160 degrees.

4. Conclusions

In this study four solvents were studied through computational methods, namely, quantum mechanics calculation and classic molecular dynamics simulations, and compared regarding their potential applications in electrochemistry. Dimethyl carbonate and trimethyl phosphate appear to be optimal to study with these methods, as they showed good results when compared to the literature and posed little to no problems during the simulations. Propylene carbonate created some problems, because of its cyclical nature and presence of a chiral centre which makes modelling it harder. Fluorinated 1,4-dimethoxybutane is a comparably bigger molecule and has been less studied which makes it more difficult to compare to experimental data. Overall, good reproducibility of literature experimental data was obtained for most of the solvents and thermodynamic properties with the used force fields. Yet, rather poor performance of the force fields in some dynamic properties, especially, for less studied solvents was achieved. This might be improved with more experimental studies, as well as with the refinement of existing force fields.

With regards to the dynamic properties obtained in this study the increase in salt concentration in these solutions led to lower values of conductivity, but higher values of viscosity, dielectric constant, and self-diffusion. These trends combined show that systems with a higher concentration of salt present worse conditions in terms of electrochemical potential, but there is a big gain in safety, which is worth the trade-off. At the same time, the most promising seems to be systems based on DMC solvent, which exhibits properties in line with those required for safe and high-energy electrical storage devices.

In terms of the structure of the systems, the interactions between Li^+ cations and the other molecules in the system were observed to be the most impactful, with the solvent being the closest in the systems containing DMC and TMP, and the anion assuming that position in the systems with PC and FDMB. Atomically, the most important relationships were established between Li and the oxygen atoms of solvents and anion. The increase in concentration did not change positions for atoms or molecules in relation to each other but did increase density of both of those in each coordination layer.

Finally, the interface between charged and uncharged graphene electrodes and the solution was studied. The effect of the charge on the interface was shown to be significant, as the negative charged electrode attracted the Li cations and repelled the anions. The contrary effect was noticed on the positively charged anode. The tilt axis probability distribution showed that anions assume the same position relative to the electrodes in all systems, while the solvent molecules show some differences, with the plane of PC

positioning itself parallelly to the normal vector of the electrode and the vectors chosen for the other solvents being perpendicular to that normal vector in z-direction.

In future, it is of great interest to study these systems with regard to their differential capacitance, as this is an important property for the use of these solvents in electrochemical storage and transformation devices. Furthermore, these systems can also be studied in a wider charge range, in order to deepen the knowledge of how they react in higher potential environments.

5. References

1. *Battery Market Size, Share & Trends Analysis Report By Product (Lead Acid, Li-ion, Nickle Metal Hydride, Ni-cd), By Application (Automotive, Industrial, Portable), By Region, And Segment Forecasts, 2020 - 2027*; Grand View Research.

2. Corporation, G. Y. *GS Yuasa Report 2021*; GS Yuasa Corporation: 2021.

3. IANS, China's BYD Auto pips Tesla to become top-selling EV brand globally. *Business Standard* 30th of August 2022, 2022.

4. Shine, I., The world needs 2 billion electric vehicles to get to net zero. But is there enough lithium to make all the batteries? *World Economic Forum* **2022**.

5. Lee, S. Y., Note 7 fiasco could burn a $17 billion hole in Samsung accounts. *Reuters* 2016.

6. Piglowska, M.; Kurc, B.; Galinski, M.; Fuc, P.; Kaminska, M.; Szymlet, N.; Daszkiewicz, P., Challenges for Safe Electrolytes Applied in Lithium-Ion Cells-A Review. *Materials (Basel)* **2021,** *14* (22).

7. Li, Q.; Chen, J. E.; Fan, L.; Kong, X. Q.; Lu, Y. Y., Progress in electrolytes for rechargeable Li-based batteries and beyond. *Green Energy Environ* **2016,** *1* (1), 18-42.

8. Suo, L. M.; Hu, Y. S.; Li, H.; Armand, M.; Chen, L. Q., A new class of Solvent-in-Salt electrolyte for high-energy rechargeable metallic lithium batteries. *Nat Commun* **2013,** *4*.

9. Zeng, Z. Q.; Murugesan, V.; Han, K. S.; Jiang, X. Y.; Cao, Y. L.; Xiao, L. F.; Ai, X. P.; Yang, H. X.; Zhang, J. G.; Sushko, M. L.; Liu, J., Non-flammable electrolytes with high salt-to-solvent ratios for Li-ion and Li-metal batteries. *Nat Energy* **2018,** *3* (8), 674-681.

10. Roy, K.; Kar, S.; Das, R. N., Computational Chemistry. In *Understanding the Basics of QSAR for Applications in Pharmaceutical Sciences and Risk Assessment*, 2015; pp 151-189.

11. Hospital, A.; Goni, J. R.; Orozco, M.; Gelpi, J. L., Molecular dynamics simulations: advances and applications. *Adv Appl Bioinform Chem* **2015,** *8*, 37-47.

12. van Duin, A. C. T.; Dasgupta, S.; Lorant, F.; Goddard, W. A., ReaxFF: A reactive force field for hydrocarbons. *J Phys Chem A* **2001,** *105* (41), 9396-9409.

13. Yang, X. H.; Zhuang, Y. B.; Zhu, J. X.; Le, J. B.; Cheng, J., Recent progress on multiscale modeling of electrochemistry. *Wires Comput Mol Sci* **2022,** *12* (1).

14. Jorgensen, W. L., Optimized Intermolecular Potential Functions for Liquid Alcohols. *J Phys Chem-Us* **1986,** *90* (7), 1276-1284.

15. Jorgensen, W. L.; Maxwell, D. S.; TiradoRives, J., Development and testing of the OPLS all-atom force field on conformational energetics and properties of organic liquids. *J Am Chem Soc* **1996,** *118* (45), 11225-11236.

16. Kreutzberger, C. B., Chloroformates and Carbonates. In *Kirk-Othmer Encyclopedia of Chemical Technology*, John Wiley & Sons, Inc.: 2001.

17. Zeng, G. F.; Xiong, S. L.; Qian, Y. T.; Ci, L. J.; Feng, J. K., Non-Flammable Phosphate Electrolyte with High Salt-to-Solvent Ratios for Safe Potassium-Ion Battery. *J Electrochem Soc* **2019,** *166* (6), A1217-A1222.

18. Yu, Z.; Wang, H. S.; Kong, X.; Huang, W.; Tsao, Y. C.; Mackanic, D. G.; Wang, K. C.; Wang, X. C.; Huang, W. X.; Choudhury, S.; Zheng, Y.; Amanchukwu, C. V.; Hung, S. T.; Ma, Y. T.; Lomeli, E. G.; Qin, J.; Cui, Y.; Bao, Z. N., Molecular design for electrolyte solvents enabling energy-dense and long-cycling lithium metal batteries. *Nat Energy* **2020,** *5* (7), 526-533.

19. Frisch, M. J. T., G. W.; Schlegel, H. B.; Scuseria, G. E.; Robb, M. A.; Cheeseman, J. R.; Scalmani, G.; Barone, V.; Petersson, G. A.; Nakatsuji, H.; Li, X.; Caricato, M.; Marenich, A. V.; Bloino, J.; Janesko, B. G.; Gomperts, R.; Mennucci, B.; Hratchian, H. P.; Ortiz, J. V.; Izmaylov, A. F.; Sonnenberg, J. L.; Williams-Young, D.; Ding, F.; Lipparini, F.; Egidi, F.; Goings, J.; Peng, B.; Petrone, A.; Henderson, T.; Ranasinghe, D.; Zakrzewski, V. G.; Gao, J.; Rega, N.; Zheng, G.; Liang, W.; Hada, M.; Ehara, M.; Toyota, K.; Fukuda, R.; Hasegawa, J.; Ishida, M.; Nakajima, T.; Honda, Y.; Kitao, O.; Nakai, H.; Vreven, T.; Throssell, K.; Montgomery, J. A., Jr.; Peralta, J. E.; Ogliaro, F.; Bearpark, M. J.; Heyd, J. J.; Brothers, E. N.; Kudin, K. N.; Staroverov, V. N.; Keith, T. A.; Kobayashi, R.; Normand, J.; Raghavachari, K.; Rendell, A. P.; Burant, J. C.; Iyengar, S. S.; Tomasi, J.; Cossi, M.; Millam, J. M.; Klene, M.; Adamo, C.; Cammi, R.; Ochterski, J. W.; Martin, R. L.; Morokuma, K.; Farkas, O.; Foresman, J. B.; Fox, D. J., Gaussian 09, Revision C.01. Gaussian Inc.: Wallingford CT, 2016.

20. Bekker, H.; Berendsen, H. J. C.; Dijkstra, E. J.; Achterop, S.; Vondrumen, R.; Vanderspoel, D.; Sijbers, A.; Keegstra, H.; Reitsma, B.; Renardus, M. K. R., Gromacs - a Parallel Computer for Molecular-Dynamics Simulations. *Physics Computing '92* **1993**, 252-256.

21. Nerut, E. R.; Karu, K.; Voroshylova, I. V.; Kirchner, K.; Kirchner, T.; Fedorov, M. V.; Ivanistsev, V. B., NaRIBaS-A Scripting Framework for Computational Modeling of Nanomaterials and Room Temperature Ionic Liquids in Bulk and Slab. *Computation* **2018,** *6* (4).

22. Martinez, L.; Andrade, R.; Birgin, E. G.; Martinez, J. M., PACKMOL: A Package for Building Initial Configurations for Molecular Dynamics Simulations. *J Comput Chem* **2009,** *30* (13), 2157-2164.

23. Berendsen, H. J. C.; Postma, J. P. M.; Vangunsteren, W. F.; Dinola, A.; Haak, J. R., Molecular-Dynamics with Coupling to an External Bath. *J Chem Phys* **1984,** *81* (8), 3684-3690.

24. Parrinello, M.; Rahman, A., Polymorphic Transitions in Single-Crystals - a New Molecular-Dynamics Method. *J Appl Phys* **1981,** *52* (12), 7182-7190.

25. Nose, S., A Molecular-Dynamics Method for Simulations in the Canonical Ensemble. *Mol Phys* **1984,** *52* (2), 255-268.

26. Hoover, W. G., Canonical Dynamics - Equilibrium Phase-Space Distributions. *Phys Rev A* **1985,** *31* (3), 1695-1697.

27. Larsen, A. H.; Mortensen, J. J.; Blomqvist, J.; Castelli, I. E.; Christensen, R.; Dulak, M.; Friis, J.; Groves, M. N.; Hammer, B.; Hargus, C.; Hermes, E. D.; Jennings, P. C.; Jensen, P. B.; Kermode, J.; Kitchin, J. R.; Kolsbjerg, E. L.; Kubal, J.; Kaasbjerg, K.; Lysgaard, S.; Maronsson, J. B.; Maxson, T.; Olsen, T.; Pastewka, L.; Peterson, A.; Rostgaard, C.; Schiotz, J.; Schutt, O.; Strange, M.; Thygesen, K. S.; Vegge, T.; Vilhelmsen, L.; Walter, M.; Zeng, Z. H.; Jacobsen, K. W., The atomic simulation environment-a Python library for working with atoms. *J Phys-Condens Mat* **2017,** *29* (27).

28. Bussi, G.; Donadio, D.; Parrinello, M., Canonical sampling through velocity rescaling. *J Chem Phys* **2007,** *126* (1).

29. Britannica, T. E. o. E., viscosity. In *Encyclopedia Britannica*, 2022.

30. Palmer, B. J., Transverse-Current Autocorrelation-Function Calculations of the Shear Viscosity for Molecular Liquids. *Phys Rev E* **1994,** *49* (1), 359-366.

31. Wilkinson, A. D. M. a. A., self-diffusion coefficient. In *IUPAC. Compendium of Chemical Terminology*, 2nd ed.; Blackwell Scientific Publications: Oxford, 1997.

32. Britannica, T. E. o. E., enthalpy. In *Encyclopedia Britannica*, 2022.

33. Sha, W.; Wu, X.; Keong, K. G., Molecular dynamics (MD) simulation of the diamond pyramid structure in electroless copper deposits. **2011**, 82-103.